High performance enrichment-based genome sequencing to support the investigation of hepatitis A virus outbreaks

Authors

Sara E. Zufan[1,2], Karolina Mercoulia[1,3], Jason Kwong[4,5], Louise M. Judd[1,6], Benjamin P. Howden[1,2,3], Torsten Seemann[1,2,3], Timothy P. Stinear[1,2]

Affiliation(s)

[1]Department of Microbiology and Immunology, The University of Melbourne at the Peter Doherty Institute for Infection and Immunity, Melbourne, VIC, Australia

[2]The Centre for Pathogen Genomics, The University of Melbourne, Melbourne, VIC, Australia

[3]Microbiological Diagnostic Unit Public Health Laboratory, The University of Melbourne, at the Peter Doherty Institute for Infection and Immunity, Melbourne, VIC, Australia

[4]Department of Infectious Diseases, Austin Health, Heidelberg, VIC, Australia

[5]Department of Infectious Diseases, The University of Melbourne at the Peter Doherty Institute for Infection and Immunity, Melbourne, VIC, Australia

[6]Doherty Applied Microbial Genomics, The University of Melbourne at the Peter Doherty Institute for Infection and Immunity, Melbourne, VIC, Australia

Corresponding author

Sara E. Zufan, s.zufan@unimelb.edu.au

Keywords

Public health genomics, culture-independent diagnostics, whole genome sequencing, food-borne surveillance, molecular epidemiology

Abstract

Hepatitis A virus (HAV) infections are an increasing public health concern in low-endemicity regions due to outbreaks from foodborne infections and sustained transmission among vulnerable groups, including persons experiencing homelessness, those who inject drugs, and men who have sex with men (MSM), which is further compounded by aging, unvaccinated populations. DNA sequence characterisation of HAV for source tracking is performed by comparing small subgenomic regions of the virus. While this approach has been successful when robust epidemiological data are available, poor genetic resolution can lead to conflation of outbreaks with sporadic cases. HAV outbreak investigations would greatly benefit from the additional phylogenetic resolution obtained by whole virus genome sequence comparisons. However, HAV genomic approaches can be difficult because of challenges in isolating the virus, low sensitivity of direct metagenomic sequencing in complex sample matrices like various foods such as fruits, vegetables and molluscs, and difficulty designing highly multiplexed PCR primers across diverse HAV genotypes. Here, we introduce a proof-of-concept pan-HAV oligonucleotide hybrid capture enrichment assay from serum and frozen berry specimens that yields complete and near-complete HAV genomes from as few as four input HAV genome copies. We used this method to recover HAV genomes from human serum specimens with high Cτ values (34·7—42·7), with high assay performance for all six human HAV sub-genotypes, both contemporary and historical. Our approach provides a highly sensitive and streamlined workflow for HAV WGS from diverse sample types, that can be the basis for harmonised and high-resolution molecular epidemiology during HAV outbreak surveillance.

Importance

This proof-of-concept study introduces a hybrid capture oligo panel for whole genome sequencing (WGS) of all six human pathogenic hepatitis A virus (HAV) subgenotypes, exhibiting a higher sensitivity than some conventional genotyping assays. The ability of hybrid capture to enrich multiple targets allows for a single, streamlined workflow, thus facilitating the potential harmonization of molecular surveillance of HAV with other enteric viruses. Even challenging sample matrices can be

53 accommodated, making it suitable for broad implementation in clinical and public health laboratories.
54 The ability to capture small amounts of virus from complex samples is promising for passive
55 surveillance application to environmental substrates, such as wastewater. This innovative approach
56 has significant implications for enhancing multijurisdictional outbreak investigations, as well as our
57 understanding of the global diversity and transmission dynamics of HAV.

Introduction

Hepatitis A is a vaccine-preventable disease caused by hepatitis A virus (HAV), a nonenveloped virus, with a small (7.5kb) positive-sense RNA genome in the family *Picornaviridae*. HAV is transmitted faecal-orally, by consuming contaminated food or drink, as well as person-to-person between close contacts.[1] It is the leading cause of acute viral hepatitis, symptoms can be prolonged but rarely result in fulminant hepatitis. Endemicity can be classified as high, intermediate, low, or very low and is generally associated with socioeconomic indicators such as hygienic and sanitary conditions.[2] Incidence of HAV infections declined in many low-endemicity countries after the implementation of routine childhood immunization by the early 2000s.[3,4] As a result, immunity in adult populations has declined significantly, thereby increasing the number of susceptible individuals who are more likely to experience and report symptoms of hepatitis.[5] Epidemiology in these regions then shifted from cyclical community wide outbreaks associated with childcare facilities or households with children, to sporadic outbreaks stemming from travellers or consumption of contaminated food from high- and intermediate-endemicity regions.[2,6–9] Another epidemiological shift began in 2016 when several North American and European countries observed a sharp increase in cases driven by person-to-person transmission, particularly in vulnerable populations including persons reporting injection drug use, experiencing homelessness, and men who have sex with men (MSM).[10–19] The combination of infection in older adults and persons with one or more comorbidities has resulted in an uptick in hospitalisations and death related to HAV infection.[5,13,20,21]

Human pathogenic HAV can be characterised into three genotypes (I, II, II), each with two subgenotypes (A, B). Distribution of subgenotypes varies geographically, although IA accounts for more than half of all reported cases.[22] Combined with epidemiological data, subgenotyping has been shown to improve outbreak characterisation and response by differentiating between sporadic and outbreak cases, determining the source of infection, and tracking chains of transmission.[17,18] Several genome regions are used for HAV genotyping. The most common regions in HAV query databases are found in or around a 168 nt fragment of the VP1/2A junction.[22–24] However, the accuracy of phylogenetic relationships inferred using these small regions has been put into question by several

85 studies that found significant variations in genetic relatedness when comparing different subgenomic
86 regions.[25–27]

87 WGS comparisons have become increasingly employed for viral surveillance and outbreak detection
88 as variation across the entire virus genome can increase the spatial and temporal phylogenetic
89 resolution of molecular epidemiology.[28] Indeed, Vaughn et al. found that subgenotyping could yield
90 misleading transmission interpretations when applied to cases with unknown epidemiological
91 associations, demonstrating that WGS was able to differentiate between sporadic and outbreak cases
92 with identical VP1/2A sequences.[27] This additional resolution could be particularly useful for guiding
93 response to growing person-to-person transmission. For example, a recent analysis of a large outbreak
94 in New York (USA) found a cluster of identical VP1/2A sequences from neighbouring jurisdictions.
95 WGS revealed 3-41 single nucleotide variants (SNVs) between cases, where the case with the greatest
96 nucleotide difference had travelled to Florida, suggesting the infection was acquired outside of the
97 local outbreak.[29,30]

98 Despite the potential benefits, WGS of HAV in a public health context has been challenging for
99 several reasons. First, HAV grows poorly in cell culture, making isolation infeasible for routine
100 culture-based WGS. Second, despite moderate genetic diversity compared to other RNA viruses,
101 enough heterogeneity across the genome exists to make it difficult to design primers for multiplex
102 amplicon sequencing.[30,31] Recently, two primer schemes for HAV WGS have been designed targeting
103 IA and/or IB, where an effort to incorporate additional subgenotypes reduced primer efficiency.[29,32]
104 Both studies had difficulty reliably recovering whole genomes from serum samples above 30 Cτ.

105 Alternatively, hybridisation capture is a highly flexible option for culture-agnostic WGS. Unlike
106 PCR-based amplification, hybrid capture reactions can contain hundreds of thousands of
107 oligonucleotide baits (probes) without interactions and are unaffected by amplification inhibitors in
108 complex sample matrices. Furthermore, conservative tiling probe design can improve the ability to
109 capture novel sequences as well as increase sensitivity in degraded samples. These characteristics
110 make it an ideal solution for routine WGS in public health laboratories for pathogens like HAV that
111 are genetically diverse and present in a variety of complex sample matrices. The flexibility of probe

design can also be leveraged to incorporate additional enteric pathogens, which can streamline library preparation and increase the sequence throughput of routine diagnostic or surveillance workflows.

Here, we present a hybridisation capture panel for undertaking WGS designed to be highly sensitive across all HAV human subgenotypes. We demonstrate the sensitivity of the capture panel to recover WGS from food (berry) and human serum samples spiked with serially diluted HAV RNA ranging from 27·9 copies/µL to below the limit of detection (LOD) (<0·2 copies/µL), corresponding to cycle threshold (Cτ) values 33·8 to >42·0. We also used the panel to recover complete and near complete (93·3%) genomes from clinical serum samples of infected patients, with and without subgenotyping data available. Finally, we used *in silico* prediction to extrapolate the efficiency of the panel to capture subgenotypes not evaluated in this study.

Materials and Methods

Pan-HAV probe design

Complete genomes of human pathogenic HAV were downloaded from GenBank on 25 Jan 2021 (N = 164). Genomes were manually selected for temporal and geographic representation of each subgenotype (N = 44). Probes were designed by IDT as previously described using a 120-mer 1X tiling approach.[33]

Optimisation experiment

Sample preparation

Food samples were prepared with frozen mixed berries according to International Organization for Standardization report ISO 15216-1:2017 with two modifications.[34] First, RNA extraction was performed on a QIASymphony with a custom protocol using the DSP Virus/Pathogen Kit with an input volume of 800 µL and elution volume of 60 µL. The second modification was the use of an Applied Biosystems 7500 Fast DX system for detection and quantification. “Low”, “mid”, and “high” virus-spiked berry specimen were prepared based on ISO 15216-2:-2019 validation studies.[35] For serum samples, ultraconcentrated spike-in material was prepared by resuspending one LENTICULE

138 disc (RM000HAV) in 222 µL PBS, followed by 10^{-1} serial dilutions in human sera. RNA extractions
139 were again performed using a QiaSymphony using the DSP Virus/Pathogen Kit with an input volume
140 of 200 µL and elution volume of 60 µL. Quantification of target copies per microliter of sample RNA
141 was performed as described in ISO 15216-1:2017. HAV LENTICULE discs were used for both the
142 quantification standards and as the spike-in material.

143 The volume of RNA extracts was equally divided to create four experimental variables: pre-
144 enrichment, pre-enrichment with concentration, post-enrichment, and post-enrichment with
145 concentration. A subset of samples were concentrated two-fold using the Zymo Clean and
146 Concentrate -5 kit including on-column DNAse treatment with a final elution volume of 10 µL. An
147 overview of the laboratory workflows are illustrated in Figure 1A.

148 **Constructing sequencing libraries**
149

150 Sequencing libraries were prepared by Illumina RNA Prep with Enrichment with 8.5 µL RNA input,
151 according to the manufacturer's protocol. Total RNA for all samples was below the recommended 10
152 ng. Briefly, RNA is synthesized to cDNA, followed by tagmentation library preparation. The indexed
153 library is then hybridized with the custom probe panel, captured, and, finally, PCR amplified. Pre-
154 enrichment controls were removed from the workflow after purification of the indexed library.
155 Enriched sample libraries were normalised to 200ng and pooled for three-plex hybridisation overnight
156 (16 hours) using the previously described pan-HAV probes (100uM). Final sequencing libraries were
157 normalised to 20nM prior to pooling for sequencing on an Illumina NextSeq2000 using a P1 2 x 150
158 bp reagent kit.

159 **Analysis of pre- and post-enrichment libraries**
160

161 Reads were adapter trimmed using cutadapt (v.2.6) with parameters -a CTGTCTCTTATACACATCT
162 -A CTGTCTCTTATACACATCT for paired-end trimming of universal dual indices.[36] Taxonomic
163 classification of trimmed reads was performed with Kraken 2 (v.2.1.2) using the viral RefSeq
164 database indexed on 05 May 2021 (available from https://benlangmead.github.io/aws-indexes/k2).[37]
165 Trimmed reads were mapped to the spike-in material reference sequence (GenBank accession

M59809.1) using minimap2 (v.2.18-r1015) with parameters -ax sr.[38,39] PCR duplicates were removed from the mapped reads using samtools *markdup* (v.1.17).[40] Mapping and quality metrics were obtained from samtools *samstats* and qualimap *bamqc* (v.2.2.2a), and collated with multiQC (v.1.14).[41,42] An overview of the bioinformatic workflows are illustrated in Figure 1B.

Application to clinical specimen

Patient samples

Archived serum samples, collected in Victoria, AUS between February and May 2023, from two infected patients were referred to the Microbiological Diagnostic Unit Public Health Laboratory for HAV WGS. A single patient had two samples taken one month apart (AUSMDU00085964, AUSMDU00085966). AUSMDU00085964 was referred with subgenotype documented as IIIA, but no subgenotype data was provided for the second referral (AUSMDU00085965). Ethical approval was granted from the University of Melbourne Human Research Ethics Committee (HREC no. 2021-22158-20072-2).

Sample preparation and sequencing

RNA extraction and quantification were performed as described earlier for serum samples. Prior to library preparation, RNA extracts were vacuum concentrated 3·7-fold for 26 minutes at ambient temperature. Library preparation was performed as described earlier in duplicate with ~7.5µL input RNA. Total RNA was below the limit of quantification by Qubit HS RNA assay. Libraries were normalised to 4nM prior to pooling for sequencing on an Illumina iSeq 100 using an i1 2 x 150bp PE reagent v2 kit.

Analysis of clinical sequences

Reads were quality controlled as described earlier. To determine the subgenotype of AUSMDU00085965, deduplicated reads were filtered to discard those that were taxonomically unclassified. Filtered reads were *de novo* assembled using SPAdes (v.3.15.5) with the rnaviral parameter enabled.[43] The longest contig was queried against a local nucleotide (nt) database of all HAV sequences available as of May 2023 from GenBank (taxon:12092) and HAVNet using BLAST

(v.2.14.0) with an e-value threshold of 10^{-4}.[44,45] The highest scoring matches belonged to subgenotype IIIA. Deduplicated reads for all samples were then mapped to the most recently available complete IIIA genome (MN062167.1) collected in 2019 from California, USA.[17] Variants were called using samtools *mpileup* and iVar *consensus* (v.1.0) with parameters -m 10 -q 30 -t 0.9.[47] Mapping and quality statistics were obtained as before. Duplicate sample reads were concatenated to create high quality consensus genomes, annotated using VADR (v.1.3), and were deposited to GenBank.[47]

Two sets of context sequences were selected for phylogenetic analysis, which were obtained by querying the individual whole genomes (*WG-query*) and the extracted VP1/2A region (*VP1/2A-query*) sequences against the local nt HAV database to retrieve the 50 highest scoring matches for each patient. These highest matching sequences to each patient were combined into a single WG-query or VP1/2A-query multifasta file and duplicate sequences were removed. Three alignments were created using MAFFT (v.7.520): WGS consensus sequences with WG-query sequences, VP1/2A consensus sequences with VP1/2A-query sequences, and WGS consensus sequences with VP1/2A-query sequences.[48] Maximum-likelihood phylogenetic tree construction was performed with IQtree (v.2.2.2.3) using the best-fit model and 1000 bootstrap replicates.[49]

In silico probe efficiency assessment

Complete and near complete (>95%; >7051nts) genomes of hepatitis A virus from human hosts were downloaded from GenBank on 24 April 2023 (N=239). Sequences used to create the probe panel were removed, with the exception of the single available IIB genome (AY644670.1), the remaining sequences were randomly subsampled to account for oversampling from outbreak studies by selecting no more than three sequences per country and year for each subgenotype using augur *filter grep* (v.21.1.0) (N=86) plus the spike-in control sequence.[50] ProbeTools (v.0.1.9) modules *capture* and *stats* were used to align the pan-HAV probe sequences against the selected target sequences to assess probe coverage and depth.[51] ProbeTools *getlowcov* was used to find low coverage regions, defined as 120-kmers with zero probe coverage at more than 40 consecutive sites. A Mann-Whitney U test was performed to evaluate whether the low probe coverage regions identified in the control sequence had

220 significantly lower read depth compared to the rest of the genome in enriched samples using scipy
221 (v.1.18.1).[52]

222 **Data Availability**

223 Complete genome sequences from AUSMDU00085964 and AUSMDU00085965 were deposited in
224 GenBank (Accessions: OR261026, OR261027). Supplementary materials, including sequencing reads
225 from the optimisation experiment, are available from https://doi.org/10.26188/23648025.

226 Results

227 Pan-HAV probe design

228 A total of 425, 120-mer biotinylated oligonucleotide probes were selected to achieve a minimum 1X
229 tiling across the representative target genomes (Supplemental Tables 1-2).

230 Optimisation experiment

231 Frozen berries and serum spiked with "high", "mid", and "low" viral genome titres of HAV RNA
232 corresponded to Cτs 35·1, 40·1, and Undetermined (<LOD) for berries, and 33·6, 36·6, and 41·0 for
233 serum, respectively (Table 1). In berries, between 0—5 unique on-target reads were detected in the
234 unenriched samples, yielding no genome coverage with a minimum read depth of 10x. In serum,
235 between 69—346 unique on-target reads were detected in unenriched samples, yielding genome
236 coverage ranging from 0—1.9% with a minimum read depth of 10.

237 An increase in read depth and genome coverage was observed in all enriched samples. After
238 enrichment of berry libraries, mean-fold enrichment increased the read depth by 315·2x in high-titre
239 samples with concentration treatment and 21·4x without; by 3·5x in mid-titre samples with
240 concentration and 7·3x without; and by 3·6x in low-titre samples with concentration and 1·3x without
241 (Figure 2A). Up to 74%, 2·3%, and <0·1% of the genome was recovered from high-, mid-, and low
242 titres at a minimum read depth of 10, respectively. Target reads were present at ≥ 1 depth up to
243 99·5%, 81·8%, and 11·7% of the genome positions in high-, mid-, and low-titre berry samples,
244 respectively (Figure 2B). After enrichment of serum libraries, mean-fold enrichment increased the

read depth by 368·9x in high-titre samples with concentration and 662·3x without; by 109·5x in mid-titre samples with concentration and 23·0x without; and by 3·1x in low-titre-samples with concentration and 3·0x without (Figure 2A). Up to 100%, 80·8%, and 10·3% of the genome was recovered from high-, mid-, and low titres using a minimum read depth of 10, respectively. Target reads were present at ≥ 1 depth up to 100%, 100%, and 91·4% of positions in high-, mid-, and low-titre serum samples, respectively (Figure 2B).

Patient samples

One patient sampled twice over a one-month period had a Cτ value of 35·8 for the first (AUSMDU00085964) and 42·7 for the second (AUSMDU00085966). AUSMDU00085965 had a Cτ value of 34·7 (Table 1). Genotyping was available for AUSMDU00085964, thus presumed for AUSMDU00085966, reported as IIIA. The genotype for AUSMDU00085965 was determined to be IIIA using the longest *de novo* assembled contig (3482nt) queried against the local HAV database. Enriched libraries of AUSMDU00085964, AUSMDU00085966, and AUSMDU00085965 were comprised of up to 12·9%, 17·2%, and 0·9% HAV classified reads (Figure 3A), yielding a mean depth up to 2455·3X, 24·3X, and 3446·4X unique target reads (Table 1), respectively. The complete genome (100%) was recovered for AUSMDU00085964 and both AUSMDU00085965 replicates, while 89·5% and 93·3% were recovered for AUSMDU00085966 replicates using a minimum read depth of 10. Target reads were present at ≥ 99·9% of genome positions in all samples (Figure 3B). Besides ambiguous bases, replicate consensus genomes were highly concordant with one discordant SNV in AUSMDU00085966.

Comparing the nucleotide differences in the WG and VP1/2A region (503 nt) between the complete sequences of both patients, there are 80 (0·011 substitutions/site) and 6 SNVs (0·012 substitutions/site), respectively. All 51 of the context sequences obtained by querying the WG sequences were >7kb, while 71·2% of the 52 context sequences obtained by querying the VP1/2A sequences were <1kb. Phylogenetic analysis of the WG sequences with WG-query context samples places the patient samples in the most recent clade descending from a clade of strains collected from India in the early 2000s (Figure 4A). Patient samples cluster together in the tree of VP1/2A sequences

with VP1/2A-query context samples amongst contemporary sequences, primarily collected in European countries (Figure4B). In the tree comparing WG sequences with VP1/2A-query context samples, patient samples are similarly found in a contemporary European clade but are distributed further apart (Figure 4C).

In silico prediction

A table of accession numbers and metadata for sequence data used for *in silico* prediction are available in Supplemental Table 3. On average, 98·6% of the queried target positions were covered by one or more probes (median 99·2, IQR 98·8—100). Subgenotypes I—IIIA and IIB are covered by one or more probes at >99·1% positions, while IB and IIIB have 97·7 and 92·8% coverage, respectively (Figure 5). Amongst strains with more than one target sequence, an average of 1·1 low probe coverage regions were identified. The single IIB and IIIB strains had zero and 5 low probe coverage regions, respectively. Three low probe coverage sites were predicted in the control sequence between positions 1690—1809, 2633—2752, and 6730—6849, none of which had significantly lower read depth compared to the rest of the genome.

Discussion

We present a hybrid capture oligo panel for WGS of all six human pathogenic HAV subgenotypes from serum and food samples, demonstrating a highly sensitive and generalized HAV WGS workflow for outbreak surveillance. This approach is a more cost-effective alternative to HAV WGS by metagenomic sequencing, can be used with degraded or challenging sample matrices, and can be employed without *a priori* genotyping.

Optimisation experiment

Enrichment of the complete HAV genome from berry specimen was observed as low as 83 input copies, and near complete (78·3%) from 4 input copies, providing the most cost-effective approach of its kind to date. Previously, deep metagenomic sequencing had recovered a near complete HAV from frozen raspberries, generating 5M reads and yielding a mean read depth of 60.[53] Lower HAV read depth observed in berry specimen compared to serum may be attributed to lower genome input copies

298 and an over fragmented library. To address the former, future optimisation should increase the input
299 volume into the concentration workflow to both remove residual inhibitors and increase input viral
300 RNA. Regarding the latter, the vigorous purification process necessary for removing inhibitors from
301 food samples resulted in nearly all sequencing libraries having average read lengths <120
302 (Supplemental Figure 1). Previous work has reported reduced hybridisation efficiency when the mean
303 insert size of the library was shorter than probe length.[54] Another possibility is residual inhibitors
304 present in the berry RNA extracts could negatively affect cDNA synthesis and tagmentation prior to
305 hybridisation, which could explain why mean-fold enrichment of cleaned and concentrated berry
306 samples was significantly greater than the untreated berry samples at high-titre. Whereas the inverse
307 was observed in lower-titres, and serum, suggesting sample loss in the spin-column outweighs the
308 benefits of purification (Figure 2A). It is recommended that future optimisation includes concentration
309 from higher input volumes to increase viral RNA input, and further determination of titres suitable for
310 column-based purification for food or other complex matrices. Additional troubleshooting is needed
311 to minimize over fragmentation during library tagmentation.

312 In serum samples, the complete genome was recovered from as few as 65 input copies, and near-
313 complete (91·4%) from 4 input copies. These results are similarly sensitive compared to amplicon-
314 based sequencing for HAV WGS from serum but offers a simplified solution for routine sequencing
315 in public health laboratories. For instance, the IA scheme presented by Lee et al. yielded a maximum
316 of 94·7% genome coverage in specimen with Cτs ranging from 27·6 to 33·3. Cleary et al. designed a
317 scheme for IA-B where nearly half of the samples with Cτ values between 16-40 yielded >=95·0%
318 genome coverage using a combination of multiplex amplicon and Sanger sequencing.[54] Previous
319 iterations of this scheme included IIA resulting in lower amplification efficiency due to the degree of
320 genetic variation between the genotypes. Unlike primer schemes for amplicon-based sequencing,
321 hybrid capture allows for the enrichment of all six subgenotypes using a pan-HAV probe panel.
322 Moreover, hybrid capture can tolerate thousands of probes, meaning additional targets can be added to
323 the current panel to facilitate robust pathogen surveillance.

Patient samples

After observing potential target loss from column-based concentration in the optimisation experiment, vacuum concentration was implemented with the clinical specimen as well as using a greater RNA extract input volume (30 μL) prior to enrichment. As a result, mean read depth and genome coverage from patient samples increased compared to contrived samples with similar Cτ values. At a minimum read depth of ten, complete genomes were recovered from AUSMDU00085964 and AUSMDU00085965, and near complete from AUSMDU00085966 (93·3%). However, 99·9% of the positions in AUSMDU00085966 were covered by one or more reads, suggesting the possibility of recovering a complete genome with greater input volume or sequencing depth. Indeed, combining reads from technical duplicates yields 97·7% coverage and 46·7 mean read depth. Regardless, such recovery at this Cτ is remarkable given the difficulty of detecting subgenotype IIIA. Recently, a reverse transcription-PCR (rRT-PCR) HAV subgenotyping assay found the LOD for IIIA to be 10 RNA copies per reaction, equivalent to 34·2 and 33·9 Cτ for singleplex and triplex reactions, respectively.[55] Whereas a subgenotype-specific optimised reverse transcription quantitative real-time PCR (RT-qPCR) assay found the limit of detection for IIIA to be 5000 copies per reaction, equivalent to Cτ near 41·3.[56] This may explain why subgenotyping data was not available for AUSMDU00085965, or typing had not been requested. Given the sensitivity observed in this study, this assay could be useful for investigating false negative cases with corroborating clinical or epidemiological evidence.

It has been demonstrated that the whole genome can provide greater geographic and temporal resolution for virus phylogenetics, generally.[28] For HAV, specifically, WGS has been shown to increase phylogenetic resolution and provide additional context in the absence of epidemiological data.[27,29] Even though substitutions per site were slightly higher in the VP1/2A region compared to the whole genome sequence (0·012 versus 0·011), phylogenetic analysis comparing whole genomes to the top VP1/2A hits provided additional resolution due to the sequences in the alignment including additional regions around the VP1/2A junction (Figure 4B-C). The previous difficulty of WGS HAV is reflected in the sequence database where few complete genomes are available, thus resulting in high

similarity to sequences more than 15 years old (Figure 4A). Until HAV genomes are better represented in these databases, it is recommended that subgenomic regions are used to select closely related sequences for phylogenetic analysis of the whole genome.

In silico prediction

We observed high capture efficiency in two of the six subgenotypes *in vitro*. Similarly, *in silico* prediction shows broad specificity across all human subgenotypes with one or more probes covered at >92% genome positions (Figure 5). Analysis of low probe coverage found an average of 1·1 120-kmer regions, representing less than 2% of the HAV genome. While low probe coverage regions were identified *in silico*, variables such as random fragmentation and hybridisation temperature can improve efficiency *in vitro*. In fact, we did not observe significantly lower read depth in regions of the enriched contrived samples where low probe coverage was predicted in the control sequence.

Limitations

This study serves as a proof-of-concept for the feasibility of a highly sensitive culture-agnostic method for HAV WGS, however, additional work is needed to further optimise and validate the approach for implementation in public health. For example, more complex sample types of public health relevance remain untested, such as stool, wastewater, or shellfish. Promising results have been found from ultra-deep sequencing of wastewater enriched with a broad viral discovery probe panel, yielding three partial HAV genomes (1482—6729nts).[57,58] Cost may also be a limiting factor for wider implementation. In the present study, the price per sample was $157AUD, approximately three-times the cost of highly multiplexed amplicon sequencing.[59] However, increased multiplexing as well as additional optimisation to increase target read proportions could lower per-sample costs. Furthermore, we anticipate the value of this approach to be the greatest for supporting food-borne surveillance, where PCR-based amplification is limited by low, degraded viral input and the presence of inhibitors.[60,61] For food specimen in particular, optimisation should evaluate the effect of pH and organic load, as well as nucleic acid shearing during virus extraction, on enrichment. Finally, overnight hybridisation was used to accommodate hands-on staffing schedules. Implementation of

377 liquid handing automation could bring the turnaround time from extraction to sequencer to under 24
378 hours.

379 Conclusion

380 This study presents, for the first time, a solitary approach for achieving highly sensitive WGS of HAV
381 from clinical and food samples, while proving relatively cost-effective. WGS of HAV can support
382 outbreak investigations by offering enhanced phylogenetic resolution and simultaneously facilitate the
383 refinement and optimisation of molecular diagnostic assays through the deposition of genome data in
384 public databases. In conclusion, flexible oligo design and hybridisation-based enrichment make this a
385 promising workflow for streamlining the surveillance of enteric viruses, thereby furthering the
386 genomic capacities of public health laboratories.

387 Acknowledgements

388 This work was supported by the National Health and Medical Research Council, Australia Partnership
389 Grant (GNT1149991) and the Australian Government Medical Research Future Fund, Genomics
390 Health Futures Mission Flagships – Pathogen Genomics Grant (FSPGN000045). SEZ is supported by
391 the Melbourne Research Scholarship from the University of Melbourne.

392 We are grateful to Dr Andrew Gador-Whyte and the Department of Microbiology at Austin Health for
393 their assistance. We thank the Victorian Infectious Disease Reference Laboratory for their valuable
394 guidance in the conceptualization of this project. We would also like to show our gratitude to Dr.
395 Ketan Patel for insightful comments on the manuscript.

396

397

Tables and Figures

					Unenriched		Enriched	
Sample	**Matrix**	**Cτ**	**Copy no. (copies/µL)**	**Concentrated**	**Mean RD**	**Coverage**	**Mean RD**	**Coverage**
BerryLow	Berry	Undet.	Undet.	N	0.0	0.0	0.2	0.0
				Y†	0.0	0.0	0.2	0.0
BerryMid		40.2	0.45	N	0.0	0.0	2.6	1.1
				Y†	0.0	0.0	2.7	2.3
BerryHigh		35.1	11.2	N	0.0	0.0	12.0	60.5
				Y†	0.1	0.0	14.8	74.1
SerumLow	Serum	41.0	0.28	N	3.1	1.9	1.2	1.0
				Y†	2.5	0.9	12.5	10.3
SerumMid		36.6	4.4	N	2.1	0.0	19.2	77.7
				Y†	2.0	0.0	28.0	80.8
SerumHigh		33.6	27.9	N	1.2	0.0	324.7	100.0
				Y†	2.3	0.6	160.7	99.6
AUSMDU00085964-1	Serum	35.8	7.1	Y‡	-	-	2455.3	100.0
AUSMDU00085964-2				Y‡	*	*	*	*
AUSMDU00085966-1		42.7	0.09	Y‡	-	-	24.3	93.3
AUSMDU00085966-2				Y‡	-	-	23.0	89.5
AUSMDU00085965-1		34.7	14.07	Y‡	-	-	3446.4	100.0
AUSMDU00085965-2				Y‡	-	-	2387.9	100.0

Table 1. Summary of sample variables and genome coverage results. Undetermined (Undet.) Cτ values occur when the target is not present or is present below the limit of detection of the assay used. Copy number is the genome copies/µL quantified from the RNA extract as determined by the ISO 15216-1 HAV quantification real-time RT-PCR protocol. Mean read depth (RD) is calculated as the average number of deduplicated reads covering one position in the

404 genome. Coverage reported here is the percentage of genome positions with a depth of 10 or more reads. A summary of positive- and negative controls can be

405 found in Supplemental Table 4.

406 [†]Zymo Clean and Concentrator -5 kit.

407 [‡]Vacuum concentration.

408 [*]No indices belonging to AUSMDU00085964-2 were identified in the sequenced reads, suggesting an error occurred during library preparatio

Figure 1. Diagram illustrating laboratory (A) and bioinformatic (B) workflows. (A) Two experiments, Optimisation and Application, were conducted involving steps such as RNA extraction from berry and/or serum samples, concentration (either column-based or vacuum), enrichment, and sequencing. Dashed arrows indicate optional steps where replicates were performed with or without the variable. (B) In the Optimisation phase, reads (shown in orange) underwent PCR duplicate filtering, mapping to a control reference, and variant calling. For the Application phase, reads (shown in pink) were filtered for PCR duplicates and target homology, followed by de novo assembly for reference selection. These filtered reads were then mapped to the chosen reference for variant calling. Diagram created using BioRender.com.

Figure 2. A) Mean-fold enrichment between paired pre- and post-enrichment samples. To avoid infinite values or overestimation using a small pseudocount, a depth of 1 was assigned to positions in pre-enriched samples where the corresponding position in the post-enriched sample was greater than 0 under the biological assumption that one or more reads must have been present for enrichment to have occurred. B) Genome coverage by spike-in titre levels at read depth thresholds of >0, ≥5, and ≥10.

Figure 3. HAV read statistics of enriched clinical specimen. A) Taxonomic classification of sample reads averaged over technical duplicates belonging to *Hepatovirus A*, non-HAV viral taxonomies, and unclassified. B) Box and whisker plot of genome coverage by sample Cτ at read depth thresholds of >0, ≥5, and ≥10.

Figure 4. Maximum likelihood trees comparing WGS- and VP1/2A-query results. Ancestral nodes were traversed to clearly visualise patient samples (blue). Nodes with high bootstrap support (≥80%) are coloured in purple. Trees were visualised using toytree (v.2.0.5).[62] A) WGS consensus sequences in the context of WG-query sequences (best-fit model = TIM2+F+I+R3). B) VP1/2A consensus sequences in the context of VP1/2A-query sequences (best-fit model = TIM2+F+I+G4). C) WGS consensus sequences in the context of VP1/2A-query sequences (best-fit model = TIM2+F+I+G4).

433 **Figure 5.** *In silico* prediction of probe efficiency, averaged by subgenotype and stratified by probe
434 coverage depth. Percentage annotation indicates the mean* predicted percent genome coverage at
435 respective probe depths.

436 *Subgenotypes IIB and IIIB each have a single genome available for comparison (AB279735.1 and
437 AY644670.1, respectively)

References

1. Koff, R. S. Hepatitis A. *Lancet* **351**, 1643–1649 (1998).
2. Shapiro, C. N. & Margolis, H. S. Worldwide epidemiology of hepatitis A virus infection. *J. Hepatol.* **18 Suppl 2**, S11-4 (1993).
3. Centers for Disease Control and Prevention. Prevention of hepatitis A through active or passive immunization: recommendations of the Advisory Commitee on Immunization Practices (ACIP). *MMWR Recomm. Rep.* (1999).
4. Advisory Committee on Immunization Practices (ACIP), Fiore, A. E., Wasley, A. & Bell, B. P. Prevention of hepatitis A through active or passive immunization: recommendations of the Advisory Committee on Immunization Practices (ACIP). *MMWR Recomm. Rep.* **55**, 1–23 (2006).
5. Klevens, R. M., Denniston, M. M., Jiles-Chapman, R. B. & Murphy, T. V. Decreasing immunity to hepatitis A virus infection among US adults: Findings from the National Health and Nutrition Examination Survey (NHANES), 1999-2012. *Vaccine* **33**, 6192–6198 (2015).
6. Bell, B. P. *et al.* The diverse patterns of hepatitis A epidemiology in the United States-implications for vaccination strategies. *J. Infect. Dis.* **178**, 1579–1584 (1998).
7. Staes, C. J. *et al.* Sources of infection among persons with acute hepatitis A and no identified risk factors during a sustained community-wide outbreak. *Pediatrics* **106**, E54 (2000).
8. Mutsch, M., Spicher, V. M., Gut, C. & Steffen, R. Hepatitis A virus infections in travelers, 1988-2004. *Clin. Infect. Dis.* **42**, 490–497 (2006).
9. Klevens, R. M. *et al.* The evolving epidemiology of hepatitis a in the United States: incidence and molecular epidemiology from population-based surveillance, 2005-2007. *Arch. Intern. Med.* **170**, 1811–1818 (2010).
10. Beebeejaun, K. *et al.* Outbreak of hepatitis A associated with men who have sex with men (MSM), England, July 2016 to January 2017. *Euro Surveill.* **22**, (2017).

11. Freidl, G. S. *et al.* Hepatitis A outbreak among men who have sex with men (MSM) predominantly linked with the EuroPride, the Netherlands, July 2016 to February 2017. *Euro Surveill.* **22**, (2017).
12. Latash, J. *et al.* Notes from the Field: Increase in Reported Hepatitis A Infections Among Men Who Have Sex with Men - New York City, January-August 2017. *MMWR Morb. Mortal. Wkly. Rep.* **66**, 999–1000 (2017).
13. Foster, M. *et al.* Hepatitis A Virus Outbreaks Associated with Drug Use and Homelessness - California, Kentucky, Michigan, and Utah, 2017. *MMWR Morb. Mortal. Wkly. Rep.* **67**, 1208–1210 (2018).
14. Friesema, I. H. *et al.* Spillover of a hepatitis A outbreak among men who have sex with men (MSM) to the general population, the Netherlands, 2017. *Euro Surveill.* **23**, (2018).
15. Ndumbi, P. *et al.* Hepatitis A outbreak disproportionately affecting men who have sex with men (MSM) in the European Union and European Economic Area, June 2016 to May 2017. *Euro Surveill.* **23**, (2018).
16. Foster, M. A. *et al.* Increase in Hepatitis A Virus Infections - United States, 2013-2018. *MMWR Morb. Mortal. Wkly. Rep.* **68**, 413–415 (2019).
17. Probert, W. S., Gonzalez, C., Espinosa, A. & Hacker, J. K. Molecular Genotyping of Hepatitis A Virus, California, USA, 2017-2018. *Emerg. Infect. Dis.* **25**, 1594–1596 (2019).
18. Haddix, M. *et al.* Use of Molecular Epidemiology to Inform Response to a Hepatitis A Outbreak - Los Angeles County, California, October 2018-April 2019. *MMWR Morb. Mortal. Wkly. Rep.* **69**, 820–824 (2020).
19. Foster, M. A. *et al.* Widespread Hepatitis A Outbreaks Associated with Person-to-Person Transmission - United States, 2016-2020. *MMWR Morb. Mortal. Wkly. Rep.* **71**, 1229–1234 (2022).
20. Batdorf, S. J. *et al.* Estimated Medicaid Costs Associated with Hepatitis A During an Outbreak - West Virginia, 2018-2019. *MMWR Morb. Mortal. Wkly. Rep.* **70**, 269–272 (2021).

21. Helmick, M. J., Morrow, C. B., White, J. H. & Bordwine, P. Widespread Community Transmission of Hepatitis A Virus Following an Outbreak at a Local Restaurant - Virginia, September 2021-September 2022. *MMWR Morb. Mortal. Wkly. Rep.* **72**, 362–365 (2023).
22. Kroneman, A. *et al.* Usability of the international HAVNet hepatitis A virus database for geographical annotation, backtracing and outbreak detection. *Euro Surveill.* **23**, (2018).
23. Robertson, B. H. *et al.* Genetic relatedness of hepatitis A virus strains recovered from different geographical regions. *J. Gen. Virol.* **73 (Pt 6)**, 1365–1377 (1992).
24. Nainan, O. V. *et al.* Hepatitis a molecular epidemiology in the United States, 1996-1997: sources of infection and implications of vaccination policy. *J. Infect. Dis.* **191**, 957–963 (2005).
25. Costa-Mattioli, M. *et al.* Genetic variability of hepatitis A virus. *J. Gen. Virol.* **84**, 3191–3201 (2003).
26. Costa-Mattioli, M. *et al.* Molecular evolution of hepatitis A virus: a new classification based on the complete VP1 protein. *J. Virol.* **76**, 9516–9525 (2002).
27. Vaughan, G. *et al.* Genetic relatedness among hepatitis A virus strains associated with food-borne outbreaks. *PLoS One* **8**, e74546 (2013).
28. Dudas, G. & Bedford, T. The ability of single genes vs full genomes to resolve time and space in outbreak analysis. *BMC Evol. Biol.* **19**, 232 (2019).
29. Cleary, N. G., Bryant, P. W., Lamson, D. M., Newman, A. P. & St George, K. A custom hepatitis A virus assay for whole-genome sequencing. *J. Virol. Methods* **312**, 114649 (2023).
30. Moratorio, G. *et al.* Bayesian coalescent inference of hepatitis A virus populations: evolutionary rates and patterns. *J. Gen. Virol.* **88**, 3039–3042 (2007).
31. Vaughan, G. *et al.* Hepatitis A virus: host interactions, molecular epidemiology and evolution. *Infect. Genet. Evol.* **21**, 227–243 (2014).
32. Lee, G.-Y. *et al.* Genotyping and Molecular Diagnosis of Hepatitis A Virus in Human Clinical Samples Using Multiplex PCR-Based Next-Generation Sequencing. *Microorganisms* **10**, (2022).
33. Bonsall, D. *et al.* ve-SEQ: Robust, unbiased enrichment for streamlined detection and whole-genome sequencing of HCV and other highly diverse pathogens. *F1000Res.* **4**, 1062 (2015).

34. International Organization for Standardization. *Microbiology of the Food Chain–Horizontal Method for Determination of Hepatitis A Virus and Norovirus Using Real-time RT-PCR- Part1: Method for Quantification*. (2017).

35. International Organization for Standardization. *Microbiology of the Food Chain-Horizontal Method for Determination of Hepatitis A Virus and Norovirus Using Real-time RT-PCR- Part2: Method for Detection*. (2019).

36. Martin, M. Cutadapt removes adapter sequences from high-throughput sequencing reads. *EMBnet J.* **17**, 10 (2011).

37. Wood, D. E., Lu, J. & Langmead, B. Improved metagenomic analysis with Kraken 2. *Genome Biol.* **20**, 257 (2019).

38. Li, H. Minimap2: pairwise alignment for nucleotide sequences. *Bioinformatics* **34**, 3094–3100 (2018).

39. Li, H. New strategies to improve minimap2 alignment accuracy. *Bioinformatics* **37**, 4572–4574 (2021).

40. Danecek, P. *et al.* Twelve years of SAMtools and BCFtools. *Gigascience* **10**, (2021).

41. Okonechnikov, K., Conesa, A. & García-Alcalde, F. Qualimap 2: advanced multi-sample quality control for high-throughput sequencing data. *Bioinformatics* **32**, 292–294 (2016).

42. Ewels, P., Magnusson, M., Lundin, S. & Käller, M. MultiQC: summarize analysis results for multiple tools and samples in a single report. *Bioinformatics* **32**, 3047–3048 (2016).

43. Prjibelski, A., Antipov, D., Meleshko, D., Lapidus, A. & Korobeynikov, A. Using SPAdes DE Novo Assembler. *Curr. Protoc. Bioinformatics* **70**, e102 (2020).

44. Altschul, S. F., Gish, W., Miller, W., Myers, E. W. & Lipman, D. J. Basic local alignment search tool. *J. Mol. Biol.* **215**, 403–410 (1990).

45. HAVNet. *National Institute for Public Health and the Environment (RIVM)* www.havnet.nl.

46. Grubaugh, N. D. *et al.* An amplicon-based sequencing framework for accurately measuring intrahost virus diversity using PrimalSeq and iVar. *Genome Biol.* **20**, 8 (2019).

47. Schäffer, A. A. *et al.* VADR: validation and annotation of virus sequence submissions to GenBank. *BMC Bioinformatics* **21**, 211 (2020).

48. Katoh, K. & Standley, D. M. MAFFT multiple sequence alignment software version 7: improvements in performance and usability. *Mol. Biol. Evol.* **30**, 772–780 (2013).

49. Nguyen, L.-T., Schmidt, H. A., von Haeseler, A. & Minh, B. Q. IQ-TREE: a fast and effective stochastic algorithm for estimating maximum-likelihood phylogenies. *Mol. Biol. Evol.* **32**, 268–274 (2015).

50. Huddleston, J. *et al.* Augur: a bioinformatics toolkit for phylogenetic analyses of human pathogens. *J. Open Source Softw.* **6**, 2906 (2021).

51. Kuchinski, K. S., Duan, J., Himsworth, C., Hsiao, W. & Prystajecky, N. A. ProbeTools: designing hybridization probes for targeted genomic sequencing of diverse and hypervariable viral taxa. *BMC Genomics* **23**, 579 (2022).

52. Virtanen, P. *et al.* SciPy 1.0: fundamental algorithms for scientific computing in Python. *Nat. Methods* **17**, 261–272 (2020).

53. Chen, H., Wang, W., Wang, S. & Hu, Y. Near-Complete Genome Sequence of a Hepatitis A Subgenotype IB Virus Isolated from Frozen Raspberries. *Microbiol Resour Announc* **8**, (2019).

54. Gnirke, A. *et al.* Solution hybrid selection with ultra-long oligonucleotides for massively parallel targeted sequencing. *Nat. Biotechnol.* **27**, 182–189 (2009).

55. Probert, W. S. & Hacker, J. K. New Subgenotyping and Consensus Real-Time Reverse Transcription-PCR Assays for Hepatitis A Outbreak Surveillance. *J. Clin. Microbiol.* **57**, (2019).

56. Coudray-Meunier, C. *et al.* Hepatitis A virus subgenotyping based on RT-qPCR assays. *BMC Microbiol.* **14**, 296 (2014).

57. Briese, T. *et al.* Virome Capture Sequencing Enables Sensitive Viral Diagnosis and Comprehensive Virome Analysis. *MBio* **6**, e01491-15 (2015).

58. Schaeffer, J., Desdouits, M., Besnard, A. & Le Guyader, F. S. Looking into sewage: how far can metagenomics help to detect human enteric viruses? *Front. Microbiol.* **14**, 1161674 (2023).

59. Gohl, D. M. *et al.* A rapid, cost-effective tailed amplicon method for sequencing SARS-CoV-2. *BMC Genomics* **21**, 863 (2020).

60. Lee, D.-Y., Cho, S.-R., Chae, S.-J., Choi, W. & Han, M.-G. Evaluation of a test method to detect hepatitis A virus in salted shellfish. *J. Food Saf.* **41**, (2021).

61. Fitzpatrick, A. H. *et al.* Amplicon-Based High-Throughput Sequencing Method for Genotypic Characterization of Norovirus in Oysters. *Appl. Environ. Microbiol.* e0216522 (2023) doi:10.1128/aem.02165-22.

62. Eaton, D. A. R. Toytree: A minimalist tree visualization and manipulation library for Python. *Methods Ecol. Evol.* **11**, 187–191 (2020).

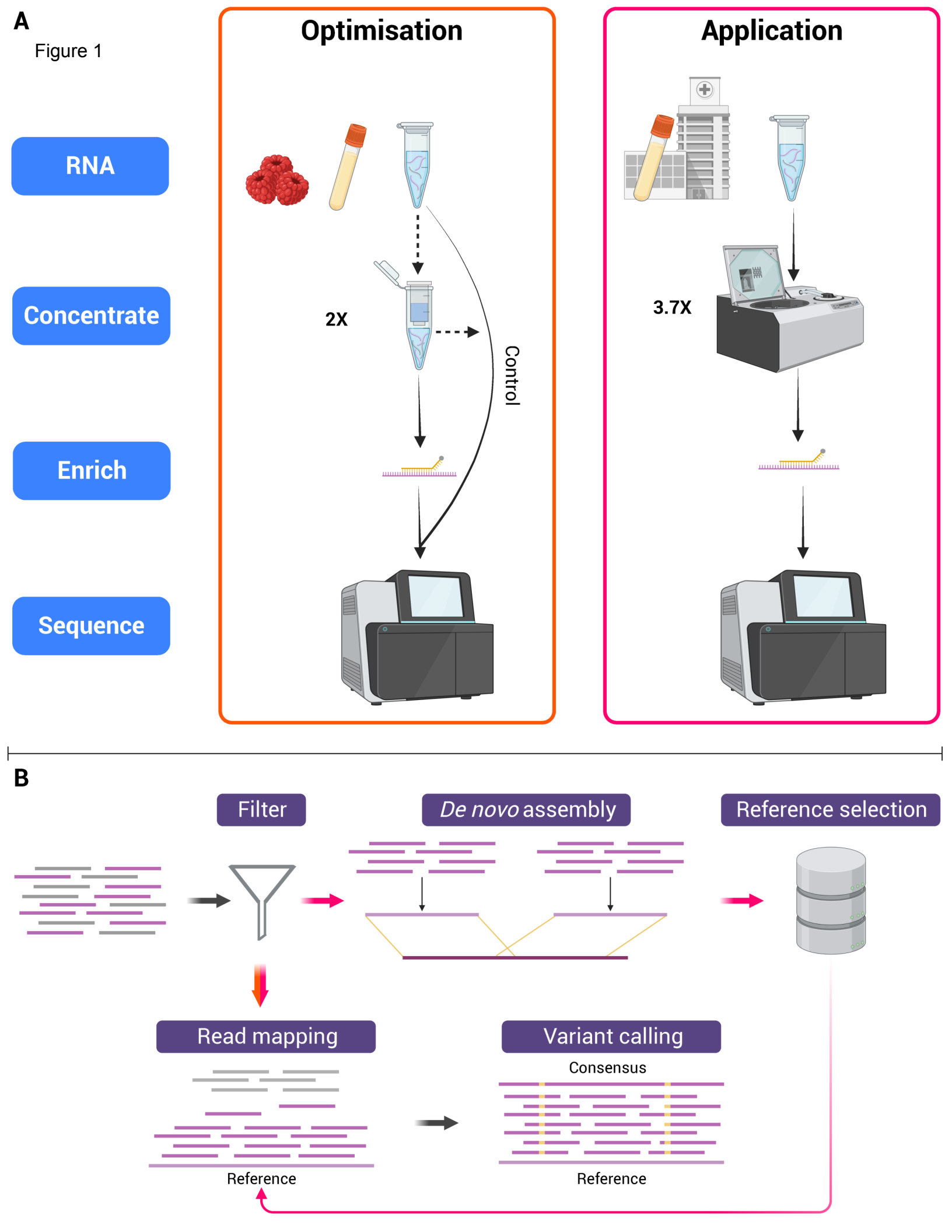
A
Figure 1
Optimisation
Application
RNA
Concentrate
Enrich
Sequence
2X
Control
3.7X
B
Filter
De novo assembly
Reference selection
Read mapping
Variant calling
Consensus
Reference
Reference

Figure 2

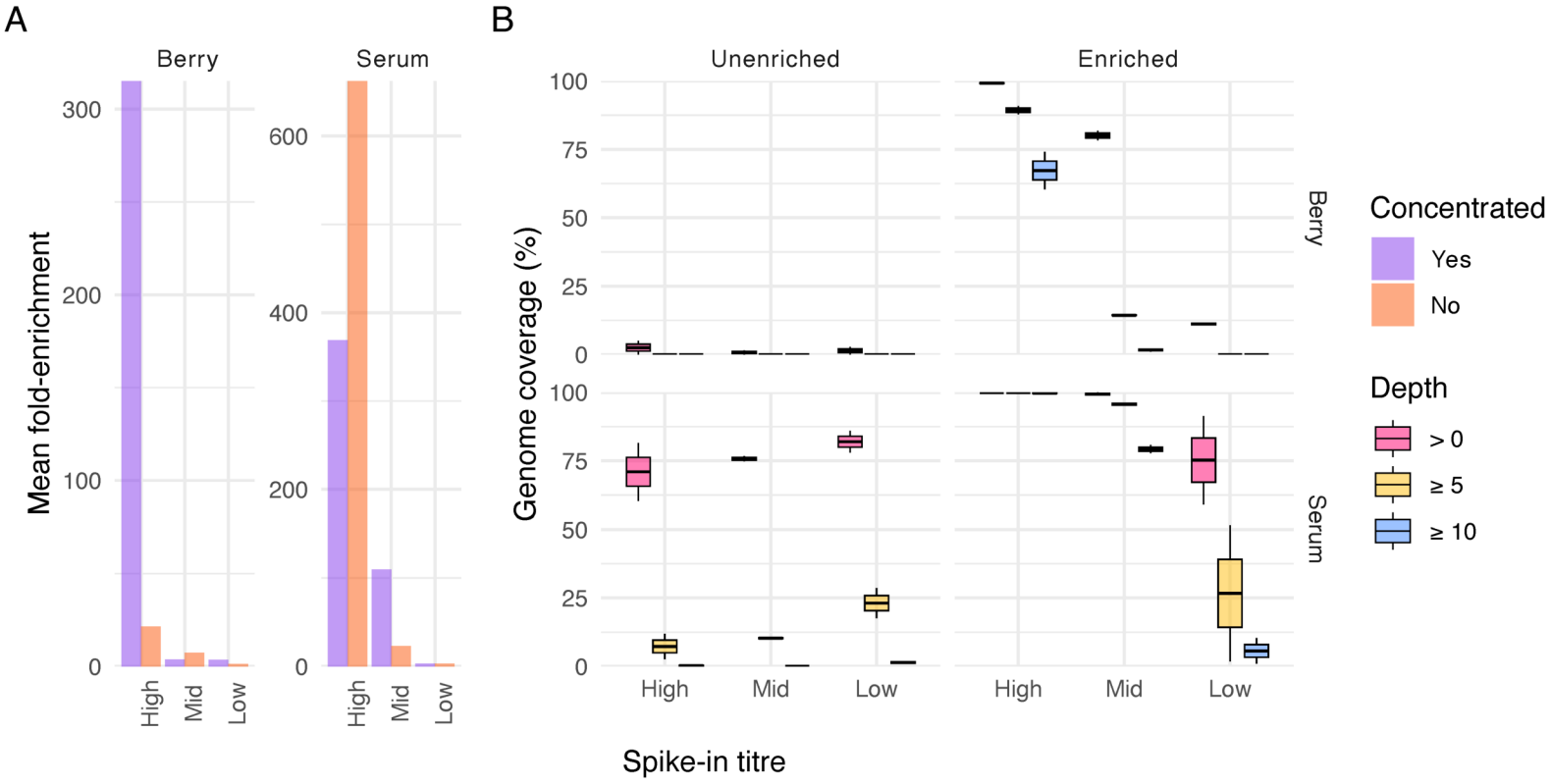
A
Berry
Serum
Mean fold-enrichment
300
200
100
0
600
400
200
0
High
Mid
Low
B
Unenriched
Enriched
Genome coverage (%)
100
75
50
25
0
Berry
Serum
Spike-in titre
Concentrated
Yes
No
Depth
> 0
≥ 5
≥ 10

Figure 3

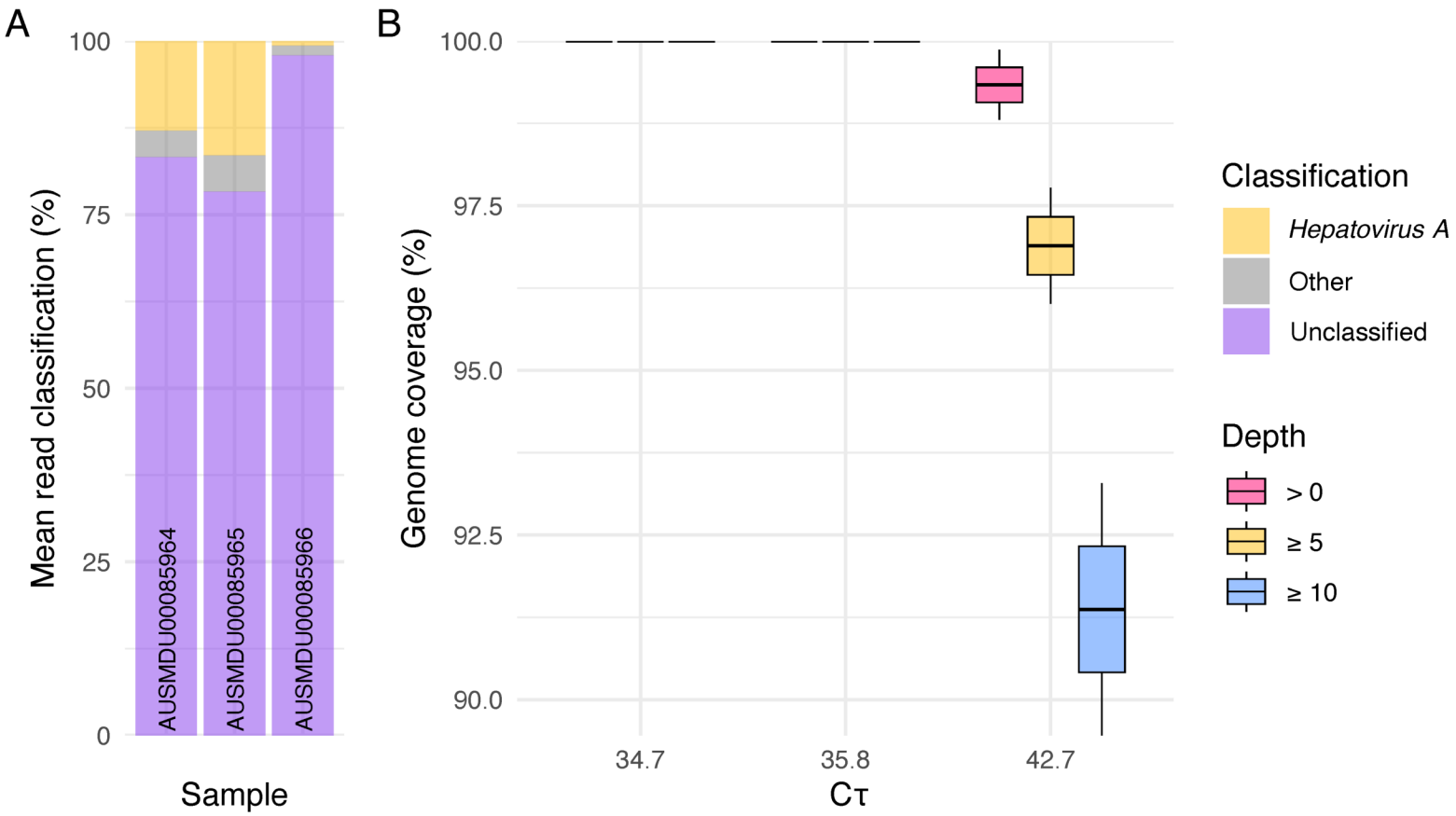
A
100
75
50
25
0
Mean read classification (%)
AUSMDU00085964
AUSMDU00085965
AUSMDU00085966
Sample
B
100.0
97.5
95.0
92.5
90.0
Genome coverage (%)
34.7
35.8
42.7
Cτ
Classification
Hepatovirus A
Other
Unclassified
Depth
> 0
≥ 5
≥ 10

Figure 4

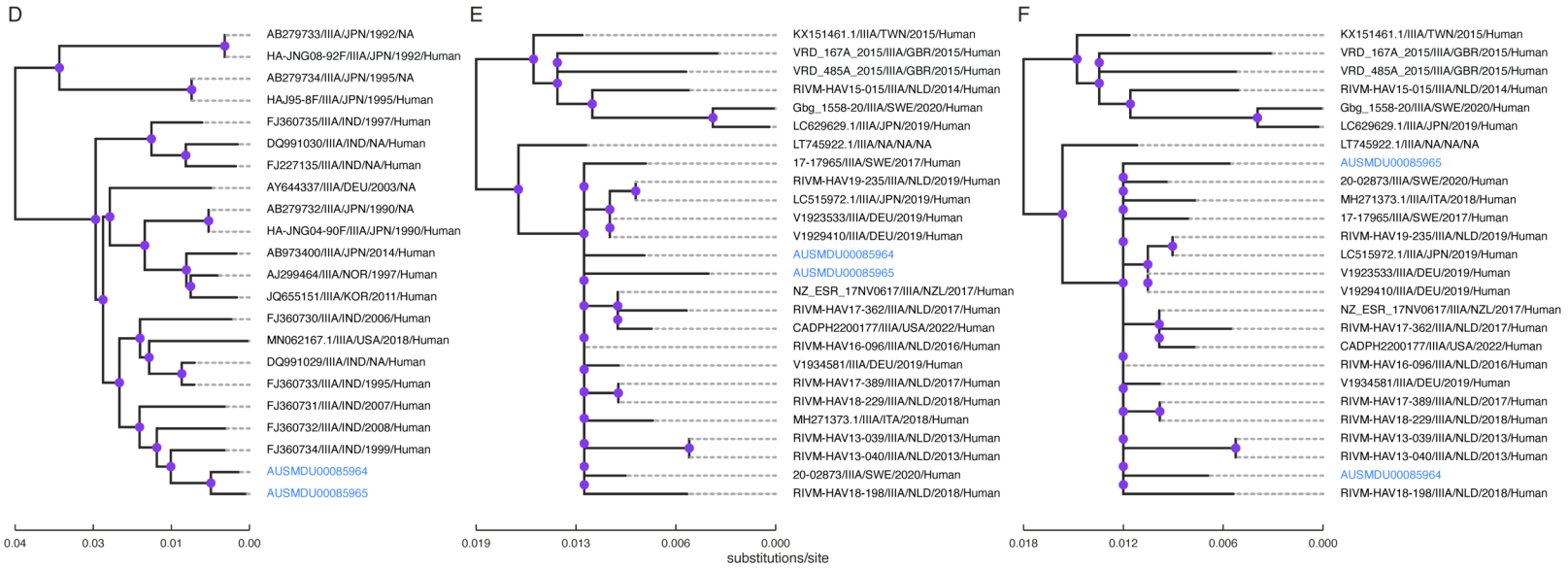
D
AB279733/IIIA/JPN/1992/NA
HA-JNG08-92F/IIIA/JPN/1992/Human
AB279734/IIIA/JPN/1995/NA
HAJ95-8F/IIIA/JPN/1995/Human
FJ360735/IIIA/IND/1997/Human
DQ991030/IIIA/IND/NA/Human
FJ227135/IIIA/IND/NA/Human
AY644337/IIIA/DEU/2003/NA
AB279732/IIIA/JPN/1990/NA
HA-JNG04-90F/IIIA/JPN/1990/Human
AB973400/IIIA/JPN/2014/Human
AJ299464/IIIA/NOR/1997/Human
JQ655151/IIIA/KOR/2011/Human
FJ360730/IIIA/IND/2006/Human
MN062167.1/IIIA/USA/2018/Human
DQ991029/IIIA/IND/NA/Human
FJ360733/IIIA/IND/1995/Human
FJ360731/IIIA/IND/2007/Human
FJ360732/IIIA/IND/2008/Human
FJ360734/IIIA/IND/1999/Human
AUSMDU00085964
AUSMDU00085965
0.04
0.03
0.01
0.00
E
KX151461.1/IIIA/TWN/2015/Human
VRD_167A_2015/IIIA/GBR/2015/Human
VRD_485A_2015/IIIA/GBR/2015/Human
RIVM-HAV15-015/IIIA/NLD/2014/Human
Gbg_1558-20/IIIA/SWE/2020/Human
LC629629.1/IIIA/JPN/2019/Human
LT745922.1/IIIA/NA/NA/NA
17-17965/IIIA/SWE/2017/Human
RIVM-HAV19-235/IIIA/NLD/2019/Human
LC515972.1/IIIA/JPN/2019/Human
V1923533/IIIA/DEU/2019/Human
V1929410/IIIA/DEU/2019/Human
AUSMDU00085964
AUSMDU00085965
NZ_ESR_17NV0617/IIIA/NZL/2017/Human
RIVM-HAV17-362/IIIA/NLD/2017/Human
CADPH2200177/IIIA/USA/2022/Human
RIVM-HAV16-096/IIIA/NLD/2016/Human
V1934581/IIIA/DEU/2019/Human
RIVM-HAV17-389/IIIA/NLD/2017/Human
RIVM-HAV18-229/IIIA/NLD/2018/Human
MH271373.1/IIIA/ITA/2018/Human
RIVM-HAV13-039/IIIA/NLD/2013/Human
RIVM-HAV13-040/IIIA/NLD/2013/Human
20-02873/IIIA/SWE/2020/Human
RIVM-HAV18-198/IIIA/NLD/2018/Human
0.019
0.013
0.006
0.000
substitutions/site
F
KX151461.1/IIIA/TWN/2015/Human
VRD_167A_2015/IIIA/GBR/2015/Human
VRD_485A_2015/IIIA/GBR/2015/Human
RIVM-HAV15-015/IIIA/NLD/2014/Human
Gbg_1558-20/IIIA/SWE/2020/Human
LC629629.1/IIIA/JPN/2019/Human
LT745922.1/IIIA/NA/NA/NA
AUSMDU00085965
20-02873/IIIA/SWE/2020/Human
MH271373.1/IIIA/ITA/2018/Human
17-17965/IIIA/SWE/2017/Human
RIVM-HAV19-235/IIIA/NLD/2019/Human
LC515972.1/IIIA/JPN/2019/Human
V1923533/IIIA/DEU/2019/Human
V1929410/IIIA/DEU/2019/Human
NZ_ESR_17NV0617/IIIA/NZL/2017/Human
RIVM-HAV17-362/IIIA/NLD/2017/Human
CADPH2200177/IIIA/USA/2022/Human
RIVM-HAV16-096/IIIA/NLD/2016/Human
V1934581/IIIA/DEU/2019/Human
RIVM-HAV17-389/IIIA/NLD/2017/Human
RIVM-HAV18-229/IIIA/NLD/2018/Human
RIVM-HAV13-039/IIIA/NLD/2013/Human
RIVM-HAV13-040/IIIA/NLD/2013/Human
AUSMDU00085964
RIVM-HAV18-198/IIIA/NLD/2018/Human
0.018
0.012
0.006
0.000

Figure 5

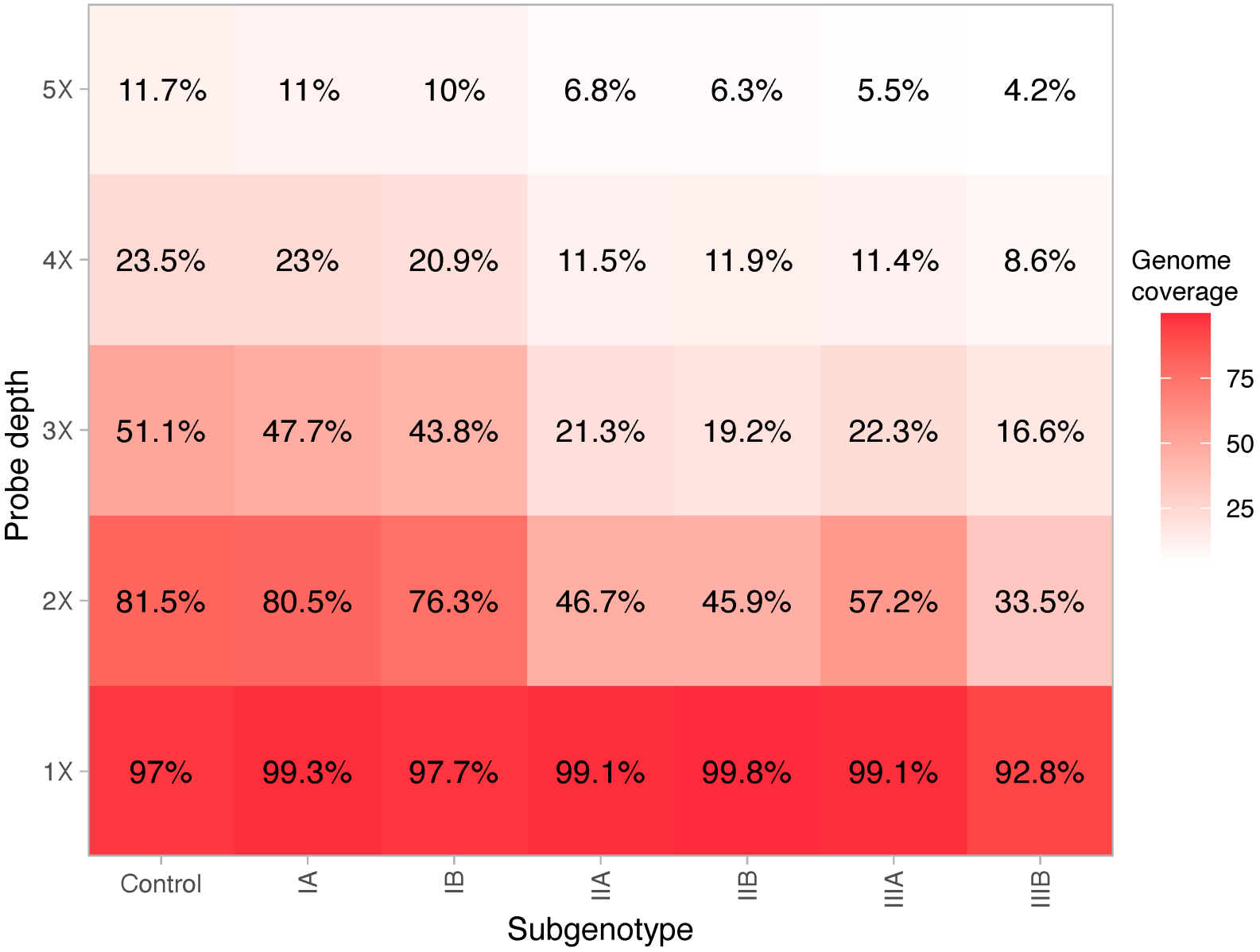
Probe depth
5X
4X
3X
2X
1X
11.7%
11%
10%
6.8%
6.3%
5.5%
4.2%
23.5%
23%
20.9%
11.5%
11.9%
11.4%
8.6%
51.1%
47.7%
43.8%
21.3%
19.2%
22.3%
16.6%
81.5%
80.5%
76.3%
46.7%
45.9%
57.2%
33.5%
97%
99.3%
97.7%
99.1%
99.8%
99.1%
92.8%
Control
IA
IB
IIA
IIB
IIIA
IIIB
Subgenotype
Genome coverage
75
50
25